mper

Experimental and Statistical Analysis of Possibility Sources – Rotation Speed, Clamping Torque and Clamping Pith for Quality Assessment in Friction Stir Welding

Ibrahim Sabry

Department of Mechanical Engineering, Faculty of Engineering, Benha University

Abstract
This paper is the first to optimize the friction stir welding (FSW) process considering the Clamp Pitch (mm) and Clamping Torque effect using the Various combinations of parameters were constructed using factorial design and responses, resulting in a comprehensive factorial analysis. Conspicuous changes in the tensile strength, yield strength, hardness, and power profile were observed for all amalgamations of parameters. Significant parameters of the FSW process have been considered in many optimization studies, however, the effect of the Clamp Pitch (mm) and Clamping Torque (Nm) has been never studied. Three levels of three parameters were used in the experiments: Clamp Pitch, tool rotational speed and Clamping Torque. The full factorial analysis was performed, was applied as an approach for selecting the values of the Significant factors of the parameters. For each result the three key parameters were important with p-values of less than 0.05, suggesting their significance in the phase of FSW. Mathematical models built with high R-sq. and least percentage error were adequate for the investigated responses. The findings were gained by important parameter values factors of 30 mm, 1800 rpm and 70 Nm for the take into consideration parameter range for the Clamp Pitch, rotational speed and Clamping Torque respectively.

Introduction

Reducing energy use is one of the greatest challenges facing modern society, particularly in the automobile and aerospace industries. This mission can be achieved by replacing the welding traditionally used with their lighter equivalents and incorporating new innovations in the welding process (Stojanovic et al., 2018; Sathari et al., 2014). A noticeable indication of this phenomenon is the widespread usage of aluminum alloys, especially in the aerospace and automotive sectors (Branco et al., 2018). Technological issues with welding therefore restrict such materials area of use. A significant number of the aluminum alloys, including 2xxx, 6xxx and 7xxx series high-strength aluminium alloys, are considered difficult to weld with

traditional methods. Those difficulties are faced with the FSW process. FSW is a process of solid-state surface alteration that induces extreme plastic deformation, material mixing, and lower exposure to temperature, resulting in substantial microstructural refining, densification, and processed layer homogeneity. Because it avoids fusion welding process faults, FSW is regarded as one of the most successful methods of combining aluminum alloys. (Gadallah et al., 2020). FSW utilizes high-speed rotating welding tools to heat the plats to allow the substance float thermoplastic and to perform weld formation under the forging action of the shaft shoulder (Guo et al., 2018). It has been described, and widely researched, as a new type of structural aerospace material at home and abroad. The weld consistency specifications are especially rigorous because of the demanding design strict.

The weld condition and the efficiency of the contact also directly impact on the structural parts and the entire piece of equipment. It is of considerable significance for the growth of the space manufacturing industry to research it in detail, considering its significant space manufacturing industry (Sabry, 2019). Because FSW requires complex interactions with sev-

Corresponding author: *Ibrahim Sabry – Department of Mechanical Engineering, Faculty of Engineering, Benha University, Benha 13518, Egypt, phone: (+2) 0100 3719 980, e-mail:* ibrahim.sabry@bhit.bu.edu.eg

eral factors that relate to the method, it is of critical importance to establish proper mathematical models for FSW which can predict the key characteristics of the method (Palanivel et al., 2011).

The effects of AA 5754 welded machine pin diameter and rotating speed at a constant welding speed on the fatigue parameters of FSW were investigated in this study (Kulekci et al., 2008). The effect of process factors on the tensile and fatigue activities of an FSW joint is detailed in this work (Barlas & Ozsarac, 2012). However, the writers did not reveal the welding specifications. The method parameters are specifically associated with plate thermal activity and then with joint mechanical properties (Sheikh-Ahmad et al., 2016). However, there are just a few reports in the literature regarding the FSW process's thermal control. The performed an experimental analysis of temperature distributions inside the work piece through FSW of aluminum alloys (Hwang et al., 2008).

Researchers are therefore attracting development of the models focused on empiric methods. Answer surface methodology (RSM) is a functional approach for evaluating, developing and optimizing structures over the parameter settings feasible domain in this regard. This approach is a set of statistical and mathematical methods, in which several variables affect an answer of response. The using RSM to build a mathematical model to estimate the FSW AA2219 aluminium alloy's corrosion resistance through the integration of FSW process parameters, used the surface response approach to build a regression model to forecast responses of the AA 2014-T6 alloy's mechanical properties of FSW (Ambabu et al., 2012; Dhancholia et al., 2014; Elatharasan & Senthil Kumar, 2013).

Welding process naturally have several responses. When trying to automate a method with many goals, various multi-objective optimization methods such as mathematical methodologies and evolutionary algorithms provide excellent results. With the methodological methods, in order to optimize UTS and reduce the corrosion reduction for FSW AA1100 Al alloys, (Periyasamy et al., 2013) used the desirability method to determine optimum conditions. With reference to metaheuristic algorithms. Various ways are practiced to UTS and hardness data of welded samples, and statistical models are used for capturing tensile test and Vickers hardness data.

Conducted an experimental investigation for modeling and parametric optimization of the FSW method in order to maximize UTS and elongation for dissimilar FSW joints of AA5052 and AISI 304 (Naghibi et al., 2016). To assess the relationship between process parameters such as machine rotational speed, welding speed, tool offset, and the aforesaid responses,

a back-propagation neural network was constructed and built.

The resulting model was then used in conjunction with a genetic algorithm to select the best process parameters (Sabry et al., 2020).

Although there are several research studies on FSW of aluminum alloy butt-joints, there are few on Clamp Pitch and Clamping Torque. The goal of this work is to evaluate the mechanical performance of friction stir welded butt-joints in an experimental setting, as well as to analyze statistically the significant parameters on responses like weld strength, power, and hardness in the nugget zone. The Response Surface Methodology (RSM) was employed to detect this region, which included 27 full factorial designs.

Finally, an appropriate model for forecasting UTS, yield strength, and hardness values of joints has been created. The model takes as inputs process parameters derived from experimental data analysis.

Experimental work

In this work, aluminum alloys (AA6061-T6) have been chosen for the FSW method to be welded to the bottom. Both plates were 5 mm thick and were cut to 100 mm long and 40 mm wide before welding. The clamp pads are aluminium bars of 10 mm AA6061-T6 used to spread the clamping force to keep the clamps from cutting into the weld plate. The anvil thick 5 mm is a 30 mm long, 60 mm broad, and 90 mm stainless steel block. The clamp plates, weld plate, and anvil are all free flowing (with no fasteners) and only with the clamping power held in position. Until every weld, they're both matched to points on the weld fixture. The weld fixture is a stainless-steel ST 304 mounted to the system table with ductile cast iron (Mohammed et al., 2015). The weld link has studs used to secure the clamps. A 100 mm long weld was run down the middle of the plate, beginning 10 mm from each side, then stopping. In this analysis, the varied parameters were clamp pitch, clamp clamping torque and tool rotation speed. Figure 1 displays the weld frame, equipped with a weld plate, with the three common clamp pitches. The FSW's weld direction is
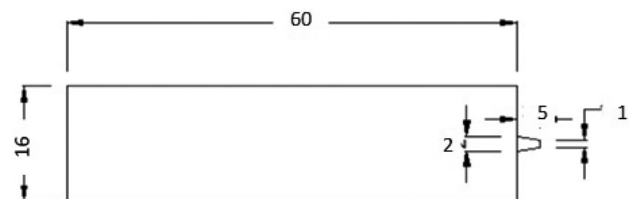

Fig. 1. Geometry of the tool design

perpendicular to the plates' rolling path. Once the experiments are begun, the mechanical properties of the base aluminium alloys, AA6061-T6, are measured. The ultimate tensile strength and yield strength of AA6061-T6 are 374 MPa and 260 MPa, respectively, and total hardness of AA606-T6, 98 VH. For use in this work, a tool made of K 100 hot work steel with a taper pin profile that was heat treated to a hardness of 60 HRC after being machined to improve its wear resistance (see Figure 2).
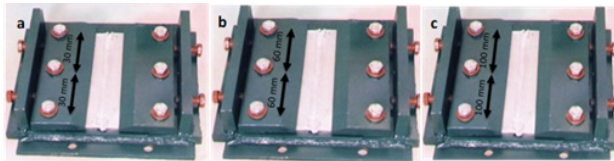

Fig. 2. Three clamp configurations used in this study: (a) clamping pitch 30 mm; (b) clamping pitch 60 mm; (c) clamping pitch 100 mm

For tensile testing, three specimens were taken from the material welds. Figure 3 presents the shape and scale of each transverse tensile specimen, and the hardness test. That analysis was carried out in compliance with the standard ASTM E8M (Sabry & El-Kassas, 2019; ASM International, 2009). care was taken through this stage to align the centre of the weld by the centre of the tensile specimen. From each FSWed joint at least three specimens were collected. The FS welded joints tensile testing was done in a reliable TTM-D (c) Zeus Ultimo Testing machine, and
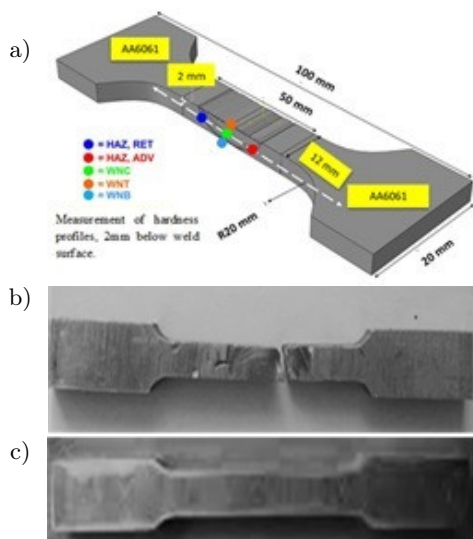

Fig. 3. Scheme of the specimens: a) Configuration and dimension of the tensile specimens and the hardness measurement; b) Weld samples after tension; c) Weld samples before tension

their tensile strength and yield strength were measured. Durability was assessed using Vickers hardness measuring equipment VM-50 in compliance with ASTME-348 (Sabry & El-Kassas, 2019; ASM International, 2009) requirements in those respective zones. Such instruments are ideal for testing the hardness of metallic components with great accuracy and a wide variety of measurements from soft to hard. To measure the minimum hardness test placed on the side of AA6061 in the HAZ regions quite close to the thermomechanically affected zone (TMAZ) in tensile tests. Micro hardness tests were done using a load of 30 Kg to determine the average minimum hardness of each joint in that area. Table 2 presented the average outcomes of the above studies.

The side where the path of spindle movement with the tool traversing is in the same path is considered the advancing line, and the returning line is considered the reverse. The parameters with a greater effect on the mechanical properties of similar FSW were selected based on the literature and previous studies, with their notations and units defined in Table 1 (Muruganandam & Das, 2011; Cole et al., 2014).

Table 1
Process parameters and their levels

Parameter	Unit	Level		
		−1	0	1
Rotational speed (N)	rpm	1000	1400	1800
Clamp Pitch (P)	mm	30	60	90
Clamping Torque (T)	Nm	40	70	100

The full factorial experiment was performed in a central composite design matrix cantered on the plan of the surface reaction, in which the three factorial design variables were chosen in three stages, consisting of 27 experimental of coded conditions, as shown in Table 2. Mathematical models have been developed to measure the FSW tensile strength, yield strength and hardness as a function of rotational speed, pitch clamping, and torque clamping. These are represented as $Y = f(N, P, T)$, where Y is the reaction, N is the speed of rotation in rpm, P is the Clamp Pitch in mm and T is the Clamping Torque in Nm. For the three variables, the chosen polynomial may be represented as:

$$Y = b0 + b1N + b2P + b3T \\ + b12N \times P + b13N \times T + b23P \times T, \quad (1)$$

where $b0$ is a constant, $b1$, $b2$, and $b3$ are linear term coefficients and $b12$, $b13$, and $b23$ are the interaction terms coefficients. The values of the polynomial

Table 2
Design matrix and experimentation for full factorial analysis

Test run	Process parameter			Experimental values			
	N (rpm)	P (mm)	T (N.M)	Power welded	Hardness	Yield strength	Tensile strength
1	−1	1	−1	105.7	81	230	345
2	−1	−1	−1	105.0	85	218	336
3	1	−1	1	106.0	83	210	327
4	−1	1	1	110.0	81	215	335
5	0	0	0	115.0	82	211	330
6	1	1	1	120.0	77	210	317
7	1	1	−1	120.2	80	212	322
8	−1	−1	1	106.0	82	210	316
9	1	1	1	120.4	77	210	317
10	−1	−1	−1	105.0	88	218	336
11	1	−1	−1	104.0	80	218	323
12	−1	−1	1	106.0	82	210	316
13	1	−1	−1	104.0	80	218	322
14	1	−1	−1	104.0	79	218	322
15	−1	−1	1	106.0	83	210	316
16	−1	1	−1	113.0	83	230	345
17	1	1	1	120.0	77	215	317
18	0	0	0	115.0	82	211	330
19	1	−1	1	120.0	80	210	327
20	1	1	−1	120.1	80	212	322
21	−1	1	−1	110.0	81	230	345
22	−1	−1	−1	105.0	85	218	336
23	−1	1	1	112.0	80	212	335
24	0	0	0	115.0	82	211	330
25	1	−1	1	120.0	80	210	327
26	1	1	−1	120.0	81	212	322
27	−1	1	1	120.0	80	215	335

equation were determined using regression analysis. Minitab program was used to statistical analysis. After the study the final mathematical models were produced in a coded form (Sabry et al., 2020; Palanivel et al., 2011; Kadaganchi et al., 2015; Sabry & Thekkuden, 2021).

Results and discussion

As seen in Figure 4, uniformly curved ripples were produced at the weld surface thanks to the tool's stirring operation in the butt joint. It arose from the shoulder's sweeping movement over the weld hunk, allowing the material to be moved from the advancing to the returning side. An unusual feature of the friction swirl welding process is the appearance of these surface ripples, often known as onion rings (Cole et al., 2014; Ahmad Shah et al., 2020; Sabry et al., 2021). No surface defects in the welded regions were found. In addition, for all samples there was no evidence of wormhole or other surface deformities in any of the joints.

Figure 5 illustrates the stress-strain relationship obtained at clamping torque 70 Nm by executing a tensile check on the butt joints. Across both experiments it has been found that the tensile strength of all butt joints is lower than the base material. For constant travel speed, the tensile strength is proportional to the rotating speed within the experimented

Fig. 4. Surface of the butt joint after the burrs are welded: (a) clamping pitch 30 mm and 1800 rpm; (b) at clamping pitch 60mm and 1800 rpm; (c) at clamping pitch 90mm and 1800 rpm
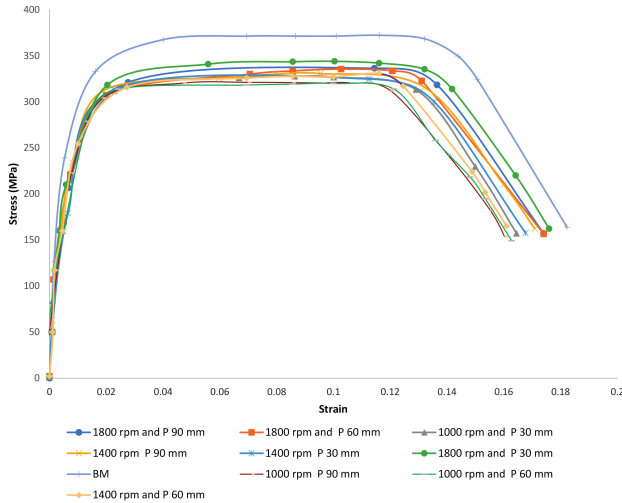

Fig. 5. Stress strain curve of welded 6061 T-6 butt joints (70 Nm clamping power). BM is base metal

range (1000 rpm to 1800 rpm). The tensile strength of the welded specimen at 1000 rpm was 325 MPa with a set clamping pitch of 30 mm which was less than 329 MPa and 345 MPa at 1400 rpm and 1800 rpm, respectively. Restriction to dislocation of grain was the cause for strong strength in certain welds prepared at 1800 rpm relative to lower rotational speed. Flash and tunnel defects in a few welds prepared at 90 mm were found. This was due to high clamping pitch (Increasing clamp width (at clamping pitch 30 mm) reduces the heat flux from the weld, by reducing the conductive cross-sectional region. It contributes to hardness and higher characteristics (which are related with greater weld temperatures and both transverse shrinkage and out of plane distortion) as well as rapid rotating tool movement across the weld line. The strength of the welds was seen to rise for clamp pitch from a low to a high value at a fixed rotational speed. For a friction stir welding operation, an optimal combination of rotational speed and clamping pitch was required to obtain a reinforced join Proper material flow and appropriate mixing. At a low clamping pitch and high rotation speed rates, the workpieces were subject to frictional heating for an extended period of time. This constant stirring of the instrument

for a long period of time at a high rotational speed can result in the development of flash defects contributing to poor joints. Nevertheless, the tensile strength was observed to be inversely proportional to rotational velocity from the tested range of clamping pitch (30 mm to 90 mm), i.e., 70 Nm clamping force had more intensity whereas 100 Nm had the least. The weld region was subjected to frictional heating only for a limited period at higher clamping power and clamping pitch, resulting in inadequate heating and weak metal material flow resulting in void creation. Such voids were usually functioning as acted as stress raisers and impacting the joint's tensile power. Figure reveals a tunnel flaw and an gap.

The thermo-mechanical FSW process can create metallurgical transformations, modifying mechanical properties, due to material movement and heat dissipation rate. Figure 6 shows a cross-section of the butt joint with a detailed optical microscopic picture depiction. The nugget region, thermal heat impacted, heat affected zone, and base metal was immediately discernible in the optical microscopic representation of the butt joint weld. Because of the atypical material distribution in the weld region, it was necessary to investigate the mechanical properties of the butt joint. The micro-hardness of the Vickers was measured in the middle portion of the transverse cross section (see Figure 7). It was observed that the strength of all the joints is smaller than that of the base material. The raw metal of microhardness measured 89 HV. maximum hardness for both clamp pitch was achieved with a mixture of fast rotation speed (1800 rpm) and fast clamping strength
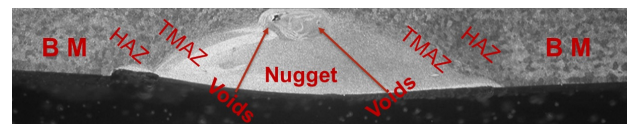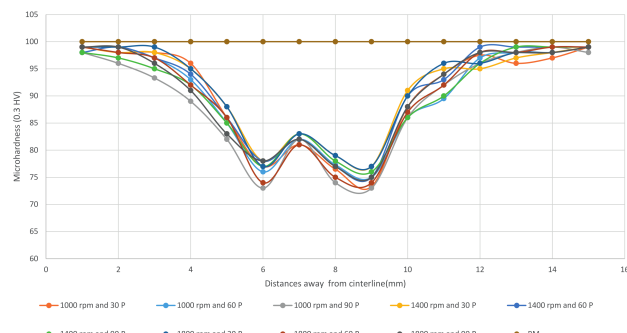

Fig. 6. Void defect in butt-joint

Fig. 7. Hardness of welded 6061-T6 samples for various rotation speed and clamping pitch (70 Nm clamping power)

(70 Nm) at various areas. Which naturally showed the metallurgical transitions in a process of friction swirl welding. Grain dislocated as a consequence, avoiding more deformation and serving as an barrier to the slide. Therefore high density of dislocation and small grains imparted high hardness and strength. Similarly, a higher rotational speed and clamp pitch at all resulted in higher hardness compared with other rotational speed and clamp pitch. The lowest hardness in the nugget zone was found in both situations as opposed to HAZ and TMAZ. Figure 7. Areas in an optical microscopic cross-sectional of the butt joint. The micro- of the Vickers was measured in the middle portion of the transverse cross section.

Developing the mathematical models

The full factorial analysis was performed based on the experimental data, taking into account the mechanical parameters of the FSW joints, such as tensile strength, yield strength, power, and hardness, as a function of rotating speed (N), clamp pith (P), and clamp torque (T). They can be expressed as seen below

$$TS \quad \text{or} \quad Ys \quad \text{or} \quad P \quad \text{or} \quad H = f(N, P, T). \quad (2)$$

In Figure 8 shows the pareto chart obtained after the full factorial analysis and present Figure 9 Normal plot standardized effect – hardness in WZ and determine significant parameter. Full factorial data obtained. Three parameters were found to be important in determining the hardness in the WZ region, namely rotational speed (N), clamp pith (P) and clamping torque (T). Hardness improved dramatically when the main effect plots seen in Figure 10 as N and P rose from their small to a high level. Notwithstanding, hardness in WZ was greater when the friction stir welding was performed at low travel level. The N, P and T p-values were 0.000, 0.000, and 0.000, respec-
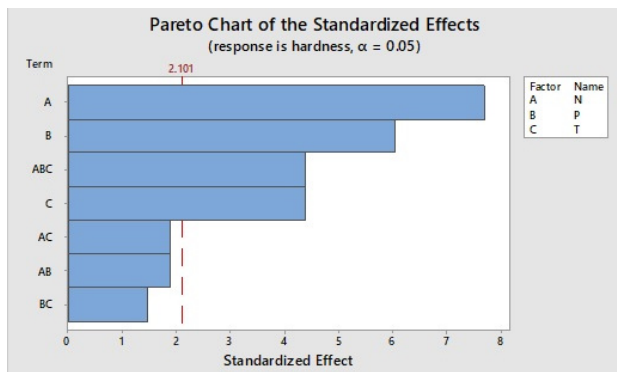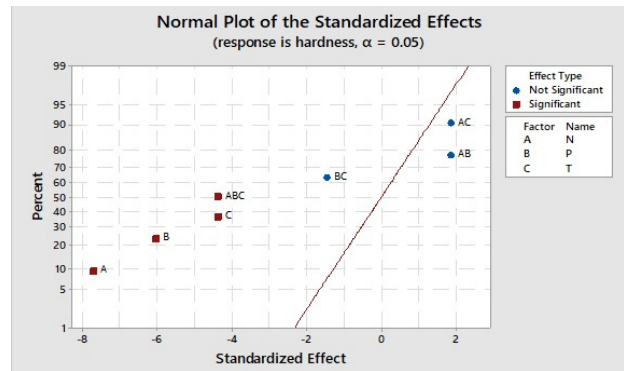

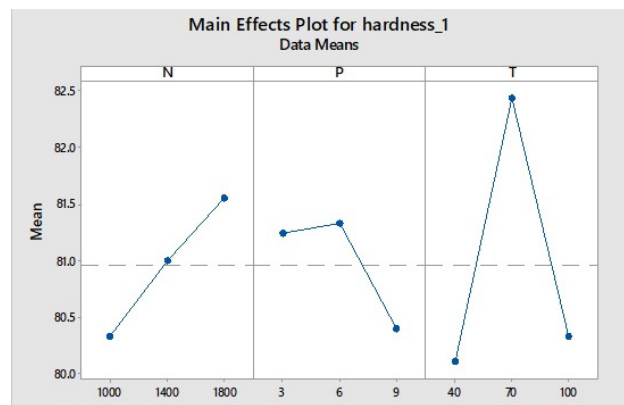Fig. 9. Normal plot standardized effect – hardness in WZ

Fig. 10. Main effects plot – hardness in WZ

tively. Since the major factors' p-values were less than 0.05, they were important in a trust interval of 95%. Interactions plot $N \times P$, $N \times T$, and $P \times T$ also had p-values of 0.078, 0.088, and 0.163, respectively. As p-values of encounters reached 0.05, they were negligible in a trust interval of 95%. The parallel lines in the interaction plot seen in Figure 11 showed insignificance of the two-way interactions. A model is given by equation (3) for predicting the hardness in
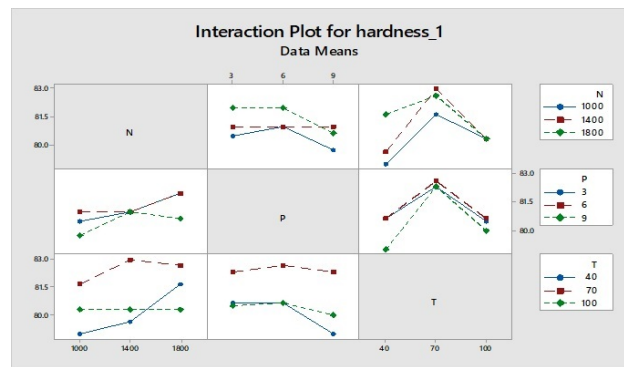

Fig. 8. Pareto chart – hardness in WZ

Fig. 11. Interaction plot – hardness in WZ

the WZ region. The model's R-sq. was 88.99%, which indicates that the variables and correlations clarified 84.09% of the variation of the hardness of the WZ as explained by the factors and interactions.

$$\begin{aligned}
\text{hardness} = {}& 81.15 + 0.4074\,A\_1000 \\
& + 0.4074\,A\_1400 - 0.8148\,A\_1800 \\
& - 0.1481\,B\_3 + 0.07407\,B\_6 + 0.07407\,B\_9 \\
& - 0.1481\,C\_40 + 0.5185\,C\_70 - 0.3704\,C\_100 \\
& + 0.5926\,A{\times}B\_1000\_3 + 1.037\,A{\times}B\_1000\_6 \\
& - 1.630\,A{\times}B\_1000\_9 - 0.4074\,A{\times}B\_1400\_3 \\
& - 0.6296\,A{\times}B\_1400\_6 + 1.037\,A{\times}B\_1400\_9 \\
& - 0.1852\,A{\times}B\_1800\_3 - 0.4074\,A{\times}B\_1800\_6 \\
& + 0.5926\,A{\times}B\_1800\_9 + 0.9259\,A{\times}C\_1000\_40 \\
& - 2.407\,A{\times}C\_1000\_70 + 1.481\,A{\times}C\_1000\_100 \\
& - 1.741\,A{\times}C\_1400\_40 + 2.593\,A{\times}C\_1400\_70 \\
& - 0.8519\,A{\times}C\_1400\_100 + 0.8148\,A{\times}C\_1800\_40 \\
& - 0.1852\,A{\times}C\_1800\_70 - 0.6296\,A{\times}C\_1800\_100 \\
& - 0.1852\,B{\times}C\_3\_40 + 0.1481\,B{\times}C\_3\_70 \\
& + 0.03704\,B{\times}C\_3\_100 + 0.5926\,B{\times}C\_6\_40 \\
& - 1.741\,B{\times}C\_6\_70 + 1.148\,B{\times}C\_6\_100 \\
& - 0.4074\,B{\times}C\_9\_40 + 1.593\,B{\times}C\_9\_70 \\
& - 1.185\,B{\times}C\_9\_100 \\
& - 0.5926\,A{\times}B{\times}C\_1000\_3\_40 \\
& + 1.741\,A{\times}B{\times}C\_1000\_3\_70 \\
& - 1.148\,A{\times}B{\times}C\_1000\_3\_100 \\
& - 1.037\,A{\times}B{\times}C\_1000\_6\_40 \\
& + 0.9630\,A{\times}B{\times}C\_1000\_6\_70 \\
& + 0.07407\,A{\times}B{\times}C\_1000\_6\_100 \\
& + 1.630\,A{\times}B{\times}C\_1000\_9\_40 \\
& - 2.704\,A{\times}B{\times}C\_1000\_9\_70 \\
& + 1.074\,A{\times}B{\times}C\_1000\_9\_100 \\
& + 1.074\,A{\times}B{\times}C\_1400\_3\_40 \\
& - 1.259\,A{\times}B{\times}C\_1400\_3\_70 \\
& + 0.1852\,A{\times}B{\times}C\_1400\_3\_100 \\
& + 0.2963\,A{\times}B{\times}C\_1400\_6\_40 \\
& + 0.6296\,A{\times}B{\times}C\_1400\_6\_70 \\
& - 0.9259\,A{\times}B{\times}C\_1400\_6\_100 \\
& - 1.370\,A{\times}B{\times}C\_1400\_9\_40 \\
& + 0.6296\,A{\times}B{\times}C\_1400\_9\_70 \\
& + 0.7407\,A{\times}B{\times}C\_1400\_9\_100 \\
& - 0.4815\,A{\times}B{\times}C\_1800\_3\_40 \\
& - 0.4815\,A{\times}B{\times}C\_1800\_3\_70 \\
& + 0.9630\,A{\times}B{\times}C\_1800\_3\_100 \\
& + 0.7407\,A{\times}B{\times}C\_1800\_6\_40 \\
& - 1.593\,A{\times}B{\times}C\_1800\_6\_70 \\
& + 0.8519\,A{\times}B{\times}C\_1800\_6\_100 \\
& - 0.2593\,A{\times}B{\times}C\_1800\_9\_40 \\
& + 2.074\,A{\times}B{\times}C\_1800\_9\_70 \\
& - 1.815\,A{\times}B{\times}C\_1800\_9\_100.
\end{aligned} \tag{3}$$

From the pareto chart for the tensile strength shown in Figure 12 and present Figure 13 normal plot standardized effect – tensile strength and determine significant parameter, N, P, T were found to be significant. The p-values were 0.000 for N, P, T. Therefore, three isolated parameters were significant to the tensile strength. The most impact plot appeared in Figure 14 validated the over deduction. P esteem of
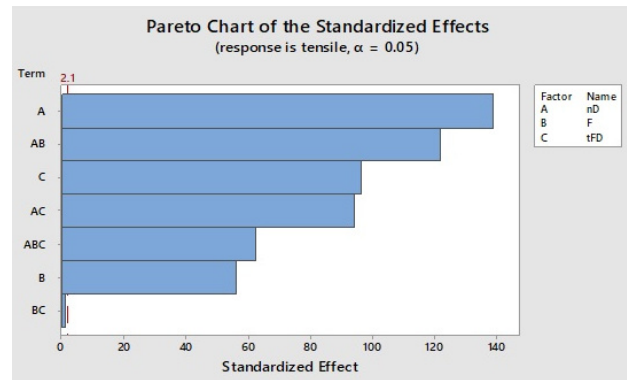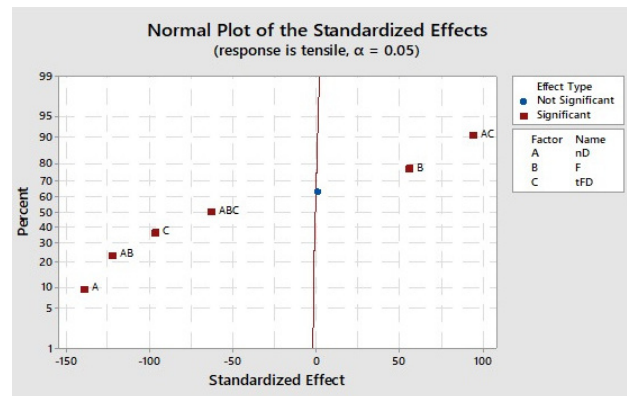

Fig. 12. Pareto chart – tensile strength

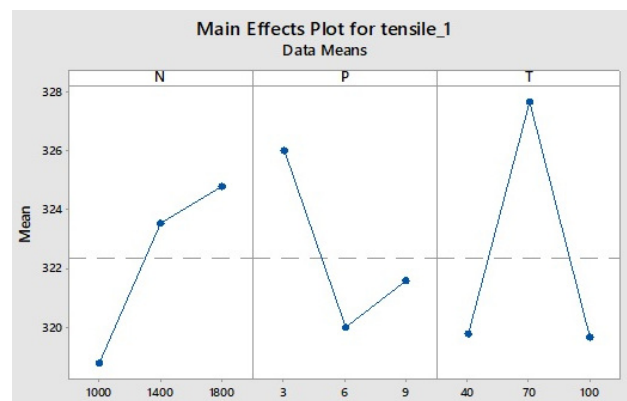Fig. 13. Normal plot standardized effect – tensile strength

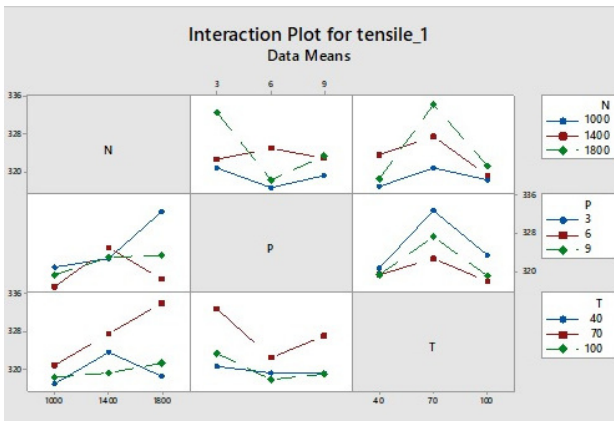Fig. 14. Tensile strength is the main effect plot

Fig. 15. WZ's interaction plot – tensile strength

two-way intelligent $N{\times}P$, $N{\times}T$, and $P{\times}T$ were 0000, 0000, and 0.303, respectively. Consequently, all the interactions were insignificant to the tensile strength, as seen in Figure 15. When the pliable quality was analysed, the tensile strength expanded when N and P changed from corresponding low to tall levels, though T changed from high to a low level. The model relating the most impacts and the interaction impacts of the parameters on tensile strength is provided by equation (4). The R-sq. of the model is 99.71%

$$\text{Tensile strength} = 327.8 + 2.852\,N\_1000$$
$$+\ 0.2963\,N\_1400 - 3.148\,N\_1800$$
$$-\ 1.704\,P\_3 - 0.3704\,P\_6 + 2.074\,P\_9$$
$$+\ 1.185\,T\_40 - 2.481\,T\_70 + 1.296\,T\_100$$
$$+\ 1.037\,N{\times}P\_1000\_3 + 5.704\,N{\times}P\_1000\_6$$
$$-\ 6.741\,N{\times}P\_1000\_9 - 4.407\,N{\times}P\_1400\_3$$
$$+\ 0.2593\,N{\times}P\_1400\_6 + 4.148\,N{\times}P\_1400\_9$$
$$+\ 3.370\,N{\times}P\_1800\_3 - 5.963\,N{\times}P\_1800\_6$$
$$+\ 2.593\,N{\times}P\_1400\_9 - 1.519\,N{\times}T\_1000\_40$$
$$-\ 3.519\,N{\times}T\_1000\_70 + 5.037\,N{\times}T\_1000\_100$$
$$-\ 1.296\,N{\times}T\_1400\_40 + 0.7037\,N{\times}T\_1400\_70$$
$$+\ 0.5926\,N{\times}T\_1400\_100 + 2.815\,N{\times}T\_1800\_40$$
$$+\ 2.815\,N{\times}T\_1800\_70 - 5.630\,N{\times}T\_1800\_100$$
$$+\ 3.370\,P{\times}T\_3\_40 - 0.9630\,P{\times}T\_3\_70$$
$$-\ 2.407\,P{\times}T\_3\_100 + 3.370\,P{\times}T\_6\_40$$
$$-\ 1.296\,P{\times}T\_6\_70 - 2.074\,P{\times}T\_6\_100$$
$$-\ 6.741\,P{\times}T\_9\_40 + 2.259\,P{\times}T\_9\_70$$
$$+\ 4.481\,P{\times}T\_9\_100$$
$$-\ 3.037\,N{\times}P{\times}T\_1000\_3\_40$$
$$+\ 6.963\,N{\times}P{\times}T\_1000\_3\_70$$
$$-\ 3.926\,N{\times}P{\times}T\_1000\_3\_100$$
$$+\ 5.963\,N{\times}P{\times}T\_1000\_6\_40$$

$$-\ 1.704\,N{\times}P{\times}T\_1000\_6\_70$$
$$-\ 4.259\,N{\times}P{\times}T\_1000\_6\_100$$
$$-\ 2.926\,N{\times}P{\times}T\_1000\_9\_40$$
$$-\ 5.259\,N{\times}P{\times}T\_1000\_9\_70$$
$$+\ 8.185\,N{\times}P{\times}T\_1000\_9\_100$$
$$+\ 1.741\,N{\times}P{\times}T\_1400\_3\_40$$
$$-\ 3.259\,N{\times}P{\times}T\_1400\_3\_70$$
$$+\ 1.519\,N{\times}P{\times}T\_1400\_3\_100$$
$$+\ 3.741\,N{\times}P{\times}T\_1400\_6\_40$$
$$+\ 2.074\,N{\times}P{\times}T\_1400\_6\_70$$
$$-\ 5.815\,N{\times}P{\times}T\_1400\_6\_100$$
$$-\ 5.481\,N{\times}P{\times}T\_1400\_9\_40$$
$$+\ 1.185\,N{\times}P{\times}T\_1400\_9\_70$$
$$+\ 4.296\,N{\times}P{\times}T\_1400\_9\_100$$
$$+\ 1.296\,N{\times}P{\times}T\_1800\_3\_40$$
$$-\ 3.704\,N{\times}P{\times}T\_1800\_3\_70$$
$$+\ 2.407\,N{\times}P{\times}T\_1800\_3\_100$$
$$-\ 9.704\,N{\times}P{\times}T\_1800\_6\_40$$
$$-\ 0.3704\,N{\times}P{\times}T\_1800\_6\_70$$
$$+\ 10.07\,N{\times}P{\times}T\_1800\_6\_100$$
$$+\ 8.407\,N{\times}P{\times}T\_1800\_9\_40$$
$$+\ 4.074\,N{\times}P{\times}T\_1800\_9\_70$$
$$-\ 12.48\,N{\times}P{\times}T\_1800\_9\_100. \qquad (4)$$

The pareto chart, normal plot standardized effect, primary impact plot, and interaction plot after the investigation considering yield strength as a reaction are appeared in Figures 16–19, respectively. N, P, T, and $P{\times}T$ with p-values 0.001, 0.000, 0.000, and 0.858 were significant. Bars within the pareto chart comparing to these components crossing the reference line equalled 2.306, also demonstrating the insignificance. Interactions of rotation speed with clamping torque and clamp pitch were not noteworthy. Within the case
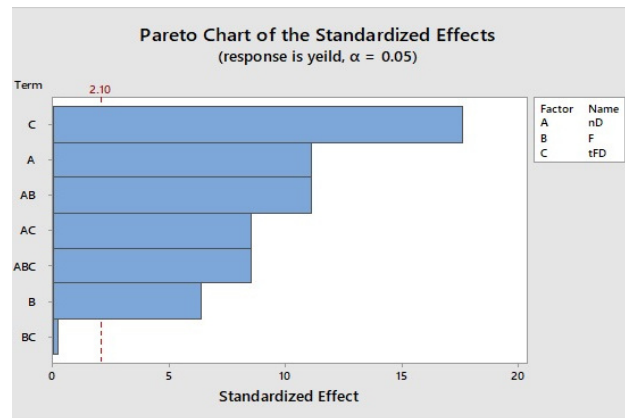

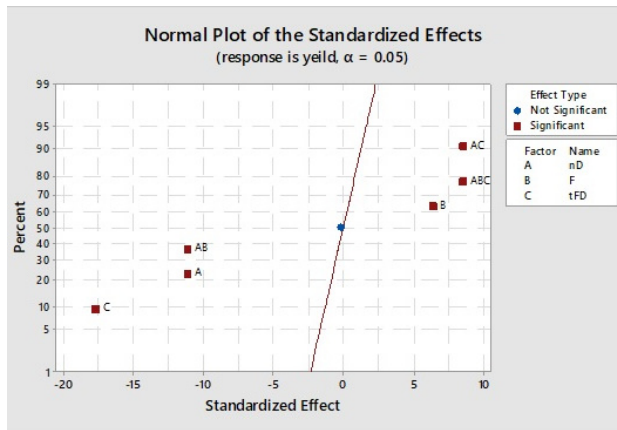Fig. 16. Pareto chart – yield strength

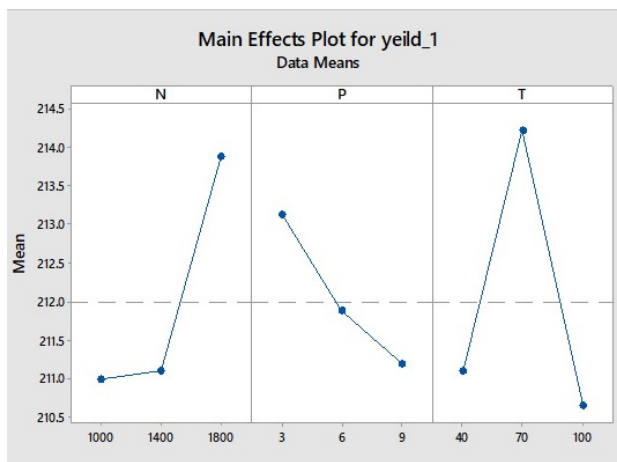Fig. 17. Normal plot standardized effect – yield strength
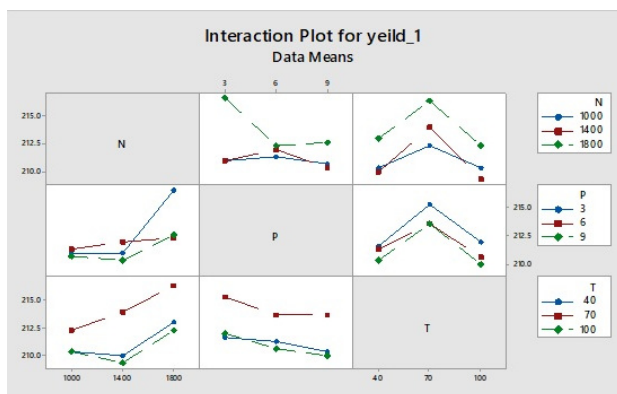

Fig. 18. Main effects plot – yield strength

Fig. 19. Interaction plot – yield strength

of yield strength, $P \times T$ interaction was furthermore critical compared to yield strength. The relapse condition of the show is given by Equation (5). The R-sq. esteem is 97.06.

$$
\begin{aligned}
\text{Yield strength} = {} & 215.0 + 0.7037\,N\_1000 \\
& + 0.7037\,N\_1400 - 1.407\,N\_1800 \\
& - 2.407\,P\_3 - 0.2963\,P\_6 + 2.704\,P\_9 \\
& - 0.4074\,T\_40 - 1.630\,T\_70 + 2.037\,T\_100 \\
& - 2.259\,N{\times}P\_1000\_3 + 3.963\,N{\times}P\_1000\_6 \\
& - 1.704\,N{\times}P\_1000\_9 - 0.5926\,N{\times}P\_1400\_3 \\
& - 3.037\,N{\times}P\_1400\_6 + 3.630\,N{\times}P\_1400\_9 \\
& + 2.852\,N{\times}P\_1800\_3 - 0.9259\,N{\times}P\_1800\_6 \\
& - 1.926\,N{\times}P\_1800\_9 + 1.741\,N{\times}T\_1000\_40 \\
& - 3.704\,N{\times}T\_1000\_70 + 1.963\,N{\times}T\_1000\_100 \\
& - 0.9259\,N{\times}T\_1400\_40 + 1.370\,N{\times}T\_1400\_70 \\
& + 2.296\,N{\times}T\_1400\_100 - 0.8148\,N{\times}T\_1800\_40 \\
& + 5.074\,N{\times}T\_1800\_70 - 4.259\,N{\times}T\_1800\_100 \\
& - 1.148\,P{\times}T\_3\_40 + 2.074\,P{\times}T\_3\_70 \\
& - 0.9259\,P{\times}T\_3\_100 + 4.074\,P{\times}T\_6\_40 \\
& - 1.370\,P{\times}T\_6\_70 - 2.704\,P{\times}T\_6\_100 \\
& - 2.926\,P{\times}T\_9\_40 - 0.7037\,P{\times}T\_9\_70 \\
& + 3.630\,P{\times}T\_9\_100 \\
& - 0.1852\,N{\times}P{\times}T\_1000\_3\_40 \\
& + 3.259\,N{\times}P{\times}T\_1000\_3\_70 \\
& - 3.074\,N{\times}P{\times}T\_1000\_3\_100 \\
& + 5.259\,N{\times}P{\times}T\_1000\_6\_40 \\
& - 2.630\,N{\times}P{\times}T\_1000\_6\_70 \\
& - 2.630\,N{\times}P{\times}T\_1000\_6\_100 \\
& - 5.074\,N{\times}P{\times}T\_1000\_9\_40 \\
& - 0.6296\,N{\times}P{\times}T\_1000\_9\_70 \\
& + 5.704\,N{\times}P{\times}T\_1000\_9\_100 \\
& - 0.1852\,N{\times}P{\times}T\_1400\_3\_40 \\
& - 1.741\,N{\times}P{\times}T\_1400\_3\_70 \\
& + 1.926\,N{\times}P{\times}T\_1400\_3\_100 \\
& - 0.07407\,N{\times}P{\times}T\_1400\_6\_40 \\
& + 2.037\,N{\times}P{\times}T\_1400\_6\_70 \\
& - 1.963\,N{\times}P{\times}T\_1400\_6\_100 \\
& + 0.2593\,N{\times}P{\times}T\_1400\_9\_40 \\
& - 0.2963\,N{\times}P{\times}T\_1400\_9\_70 \\
& + 0.03704\,N{\times}P{\times}T\_1400\_6\_100 \\
& + 0.3704\,N{\times}P{\times}T\_1800\_3\_40 \\
& - 1.519\,N{\times}P{\times}T\_1800\_3\_70 \\
& + 1.148\,N{\times}P{\times}T\_1800\_3\_100 \\
& - 5.185\,N{\times}P{\times}T\_1800\_6\_40 \\
& + 0.5926\,N{\times}P{\times}T\_1800\_3\_70 \\
& + 4.593\,N{\times}P{\times}T\_1800\_3\_100 \\
& + 4.815\,N{\times}P{\times}T\_1800\_9\_40 \\
& + 0.9259\,N{\times}P{\times}T\_1800\_9\_70 \\
& - 5.741\,N{\times}P{\times}T\_1800\_9\_100. \quad (5)
\end{aligned}
$$

The pareto chart, primary impact plot, normal plot standardized effect, and interaction plot are seen in Figures 20–23, for examination with reaction as power. Both three independent variables such as speed

of rotation, clamping pitch, and clamping torque were important for the strength. This can be seen in the pareto chart. Whereas the relationship results were not important as they remained below the degree of importance, which was 2.31. The most impact plot appeared in Figure 20 validated the over deduction. P esteem of two-way intelligent $N \times P$, $N \times T$, and $P \times T$ were 0.008, 0.156, and 0.306, respectively. Once the rotating speed was increased from 1000 rpm to
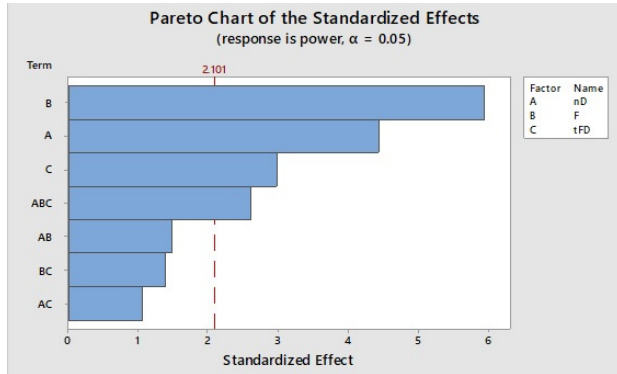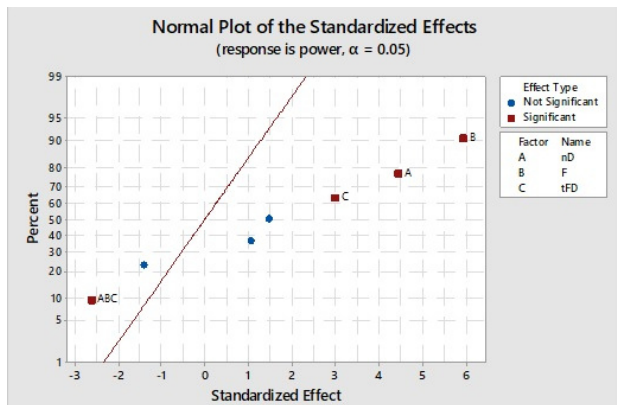

Fig. 20. Pareto chart – power

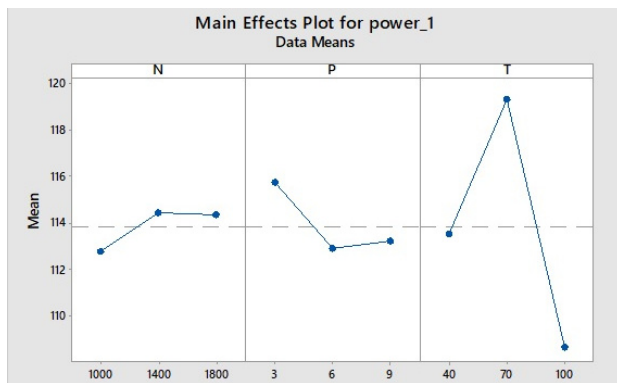Fig. 21. Normal plot standardized effect – power

Fig. 22. The main effect plot of power

1800 rpm, there was a significant improvement in the power from 105 N to 120 N. Likewise, the power of the clamp pitch was raising by 15 Nm, from 30 mm to 90 mm. The high rotational speed and clamp pitch and less clamping torque were the explanations for the power rise. The principal explanation for the increase in power was the frictional heat produced. This frictional heat produced by high rotational speed, deeper penetration, and extended touch exposure. The diagrams were identical to each other in the interaction charts, showing the insignificance of the interaction results. Equation (6) gives a logical basis for measuring power. The regression model has valued an 81.35%.

$$
\begin{aligned}
\text{Power of weld} = {} & 112.1 + 1.096\,N\_1000 \\
& - 2.026\,N\_1400 + 0.9296\,N\_1800 \\
& + 0.2185\,P\_3 + 2.341\,P\_6 - 2.559\,P\_9 \\
& - 0.3481\,T\_40 - 0.9037\,T\_70 + 1.252\,T\_100 \\
& + 1.559\,N{\times}P\_1000\_3 - 2.896\,N{\times}P\_1000\_6 \\
& + 1.337\,N{\times}P\_1000\_9 - 0.3185\,N{\times}P\_1400\_3 \\
& + 2.959\,N{\times}P\_1400\_6 - 2.641\,N{\times}P\_1400\_9 \\
& - 1.241\,N{\times}P\_1800\_3 - 0.06296\,N{\times}P\_1800\_6 \\
& + 1.304\,N{\times}P\_1800\_9 - 1.541\,N{\times}T\_1000\_40 \\
& + 6.015\,N{\times}T\_1000\_70 - 4.474\,N{\times}T\_1000\_100 \\
& + 4.915\,N{\times}T\_1400\_40 - 3.530\,N{\times}T\_1400\_70 \\
& - 1.385\,N{\times}T\_1400\_100 - 3.374\,N{\times}T\_1800\_40 \\
& - 2.485\,N{\times}T\_1800\_70 + 5.859\,N{\times}T\_1800\_100 \\
& + 3.670\,P{\times}T\_3\_40 - 3.107\,P{\times}T\_3\_70 \\
& - 0.5630\,P{\times}T\_3\_100 - 1.119\,P{\times}T\_6\_40 \\
& + 1.770\,P{\times}T\_6\_70 - 0.6519\,P{\times}T\_6\_100 \\
& - 2.552\,P{\times}T\_9\_40 + 1.337\,P{\times}T\_9\_70 \\
& + 1.215\,P{\times}T\_9\_100 \\
& - 1.781\,N{\times}P{\times}T\_1000\_3\_40 \\
& - 2.004\,N{\times}P{\times}T\_1000\_3\_70 \\
& + 3.785\,N{\times}P{\times}T\_1000\_3\_100 \\
& + 3.341\,N{\times}P{\times}T\_1000\_6\_40 \\
& + 0.4519\,N{\times}P{\times}T\_1000\_6\_70 \\
& - 3.793\,N{\times}P{\times}T\_1000\_6\_100 \\
& - 1.559\,N{\times}P{\times}T\_1000\_9\_40 \\
& + 1.552\,N{\times}P{\times}T\_1000\_9\_70 \\
& + 0.007407\,N{\times}P{\times}T\_1000\_9\_100 \\
& - 1.763\,N{\times}P{\times}T\_1400\_3\_40 \\
& + 3.541\,N{\times}P{\times}T\_1400\_3\_70 \\
& - 5.304\,N{\times}P{\times}T\_1400\_3\_100 \\
& + 1.152\,N{\times}P{\times}T\_1400\_6\_40 \\
& - 6.737\,N{\times}P{\times}T\_1400\_6\_70 \\
& + 5.585\,N{\times}P{\times}T\_1400\_3\_100 \\
& - 2.915\,N{\times}P{\times}T\_1400\_6\_40 \\
& + 3.196\,N{\times}P{\times}T\_1400\_6\_70
\end{aligned}
$$

$$- 0.2815 \, N{\times}P{\times}T\_1400\_6\_100$$
$$+ 0.01852 \, N{\times}P{\times}T\_1800\_3\_40$$
$$- 1.537 \, N{\times}P{\times}T\_1800\_3\_70$$
$$+ 1.519 \, N{\times}P{\times}T\_1800\_3\_100$$
$$- 4.493 \, N{\times}P{\times}T\_1800\_6\_40$$
$$+ 6.285 \, N{\times}P{\times}T\_1800\_6\_70$$
$$- 1.793 \, N{\times}P{\times}T\_1800\_6\_100$$
$$+ 4.474 \, N{\times}P{\times}T\_1800\_9\_40$$
$$- 4.748 \, N{\times}P{\times}T\_1800\_9\_70$$
$$+ 0.2741 \, N{\times}P{\times}T\_1800\_9\_100. \qquad (6)$$

Fig. 23. The power of interactions is plotted on a graph

Fig. 24. Using the response optimizer in ANOVA, the parameters and responses were optimized

In a 95% confidence interval, the *p*-values for all interactions, such as rotation speed, clamp pitch, and clamping torque, were less than 0.05. The importance of the interaction effect of factors on tensile strength, power, and hardness was further demonstrated by the high *F*-values. This evidently proved that the tensile strength and hardness is count on the conditions of the welding procedure. However, in order to improve the parameters, this study looks into tensile strength, yield strength, power, and hardness. Figure 24 shows the optimized parameters (rotation speed, clamp pitch and clamping torque) and the corresponding response values (tensile strength, yield strength, power welding and hardness) in ANOVA using the response optimizer. The optimal combination of parameters for a single response or a group of responses can be determined using a response optimizer. After optimizing several responses for the three input variables, an optimization plot was obtained in this scenario. 1800 rpm, 3 mm, and 70 Nm were the optimal rotation speed, clamp pitch, and clamping, respectively.
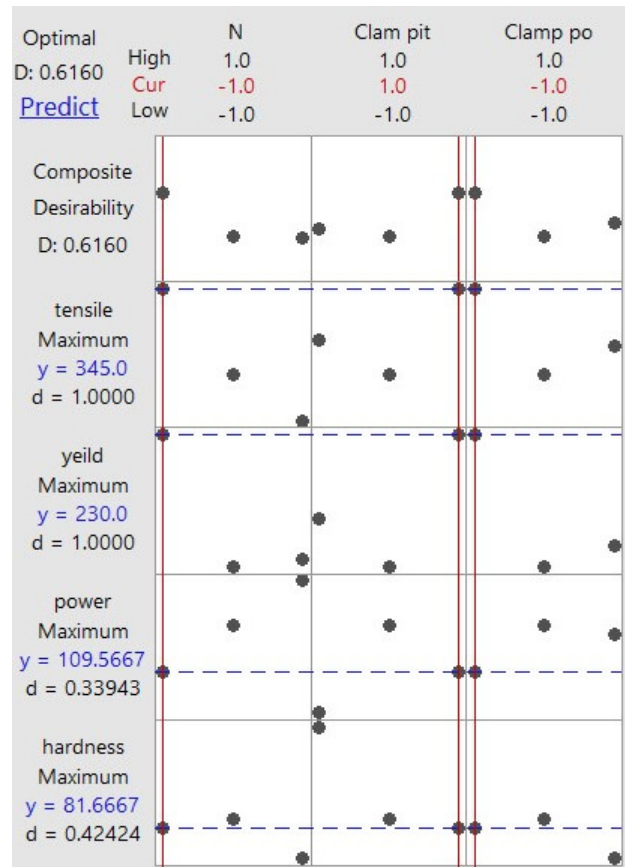
Discussion

It was revealed that the hardness, power of weld and strength in WZ had undergone changes during the rotation speed, clamp force and clamping torque. The decrease in hardness, power of weld and strength by an increase in the clamping pitch (cm) and could be explained by a number of elements working together.

Furthermore, the findings of statically analysis revealed that the FSW clamp pitch(cm) was much higher than the FSW with a lower rotation speed. As Figures 11, 15, 19 and 23 a compares, the strength in the cross-sections of the studied welds in the WZ was more than in the clamping pitch 3(cm) and clamping torque 70 (Nm) joint in comparison with clamping pitch 6 and 9(cm) and clamping torque 40 and 100 (Nm). Because clamp spacing and torque have a significantly greater impact on tensile and yield strength than they do on hardness, clamping parameters should be chosen with distortion in mind. The tensile strength, yield strength and hardness optimized weld schedule would then be 1800 rpm, clamp-

ing pitch 30 mm and clamping torque 70 Nm. Higher tensile strength was thought to facilitate grain nucleation during dynamic re-crystallization, which could explain the WZ microstructure's uniform grain distribution (Ahmed & El-Kassas, 2019; Ahmad Shah et al., 2020).

Conclusions

Using established fittings and an experimental setup, all joints were successfully friction stir welded. Tensile strength, yield strength, power and hardness in the nugget zone, of welded joints for different parameters (rotation speed, clamp pitch, and clamping torque) were assessed. During study conclusions were observed after the research investigation.

1. Within the testing range (1000 rpm to 1800 rpm) at a constant travel speed, tensile strength was related to rotational speed. The tensile strength of the material increased as the clamp pitch was reduced.
2. The samples welded at a combination of high rotational speed and high clamping torque had a rather high hardness.
3. Unless clamp torque was simply a mechanical influence, that would not have a marginal impact on nugget strength, because increasing clamp torque does not alter the temperature of the weld. Based on this discrepancy it can be concluded that the response variables are influenced by both mechanical and thermal processes.
4. Weld strength increase as rotation speed is increased. Increasing clamp width (at clamping pitch 30 mm) reduces the heat flux from the weld, by reducing the conductive cross-sectional region.
5. Because clamp spacing and torque have a significantly greater impact on tensile and yield strength than they do on hardness, clamping parameters should be chosen with distortion in mind. The tensile strength, yield strength and hardness optimized weld schedule would then be 1800 rpm, clamping pitch 30 mm and clamping torque 70 Nm.
6. The bars corresponding to important factors in the pareto map reached the point of importance. P-Values of these variables and relationships were less than 0.05 at a trust level of 95%.
7. Tensile strength, yield strength, power, and hardness in WZ had R-sq. values of 99.30 percent, 99.66 percent, 98.91 percent, 98.78 percent, and 97.07 percent, respectively. These responses had percentage errors of 0.91 percent, 1.03 percent, 1.72 percent, 2.08 percent, and 1.88 percent, respec-

tively, between actual and projected responses. The models are highly satisfying because they have a high R-sq. value and a low percentage error.

References

Ahmed, I.S., El-Kassas, M. (2019). *Optimization of the Underwater Friction Stir Welding of Pipes Using Hybrid RSM-Fuzzy Approach.* International Journal of Applied Engineering Research, 14, 24.

Ahmad Shah, L.H., Midawi, A., Walbridge, S., and Gerlich, A. (2020). *Influence of tool offsetting and base metal positioning on the material flow of AA5052-AA6061 dissimilar friction stir welding.* Journal of Mechanical Engineering and Sciences, 14, 1, 6393–6402.

Ambabu, G., Balaji Naik, D., Venkata Rao, C., Srinivasa, K.R., and Madhusudan G.R. (2015). *Optimization of friction stir welding parameters for improved corrosion resistance of AA2219 aluminum alloy joints.* Defence Technology, 11, 330–337.

ASM International (2009). Handbook Volume 2: Properties and selection: nonferrous alloys and special-purpose materials.

Barlas, Z. and Ozsarac, U. (2012). *Effects of FSW Parameters on Joint Properties of Al-Mg3 Alloy.* Welding Journal, 91, 16–22.

Branco, R., Berto, F., and Kotousov, A. (2018). *Mechanical Behaviour of Aluminium Alloys,* MDPI.

Cole, E., Fehrenbacher, A., Duffie, N., Zinn, M., Pfefferkorn, F., and Ferrier, N. (2014). *Weld temperature effects during friction stir welding of dissimilar aluminum alloys 6061-t6 and 7075-t6.* International Journal of Advanced Manufacturing Technology, 71, 643–652.

Dhancholia, D.D., Sharma, A., and Vyas, CH. (2014). *Optimisation of Friction Stir Welding Parameters for AA 6061 and AA 7039 Aluminium Alloys by Response Surface Methodology (RSM).* International Journal of Advanced Mechanical Engineering, 4, 5, 565–571.

Elatharasan, G. and Senthil Kumar, V.S. (2013). *An Experimental Analysis and Optimization of Process Parameter on Friction Stir Welding of AA 6061-T6 Aluminum Alloy using RSM.* Procedia Engineering, 64, 1227–1234.

Gadallah, N., Sabry, I., and Ghafaar M.A. (2020). *A Summarized Review on Friction Stir Welding for Aluminum Alloys.* International Journal on: The Academic Research Community Publication, IEREK Press. DOI: 10.21625/archive.v4i1.695.

Guo, S., Shah, L., Ranjan, R., Walbridge, S., and Gerlich, A. (2018). *Effect of quality control parameter variations on the fatigue performance of aluminum friction stir welded joints.* International Journal of Fatigue, 118, 150–161.

Hwang, Y., Kang, X., Chiou Y., and Hsu, H. (2008). *Experimental study on temperature distributions within the work piece during friction stir welding of aluminum alloys.* International Journal of Machine Tools and Manufacture, 48, 778–787.

Kadaganchi, R., Gankidi, M.R., and Gokhale, H. (2015). *Optimization of process parameters of aluminum alloy AA 2014-T6 friction stir welds by response surface methodology.* Defence Technology, 11, 209–219.

Kulekci, M.K., Sik, A., and Kaluc, E. (2008). *Effects of tool rotation and pin diameter on fatigue properties of friction stir welded lap joints.* The International Journal of Advanced Manufacturing Technology, 36, 877–882.

Mohammed, M.H., Ishak, M., and Rejab, R. (2015). *A simplified design of clamping system and fixtures for friction stir welding of aluminium alloys.* Journal of Mechanical Engineering and Sciences, 9, 1628–1639.

Muruganandam, D. and Das, S. (2011). *Friction Stir Welding Process Parameters for Joining Dissimilar Aluminum Alloys.* International Journal of Mechanical Engineering and Technology, 2, 25–38.

Naghibi, H., Shakeri, M., and Hosseinzadeh, M. (2016). *Neural Network and Genetic Algorithm Based Modeling and Optimization of Tensile Properties in FSW of AA 5052 to AISI 304 Dissimilar Joints.* Transactions of the Indian Institute of Metals, 69, 4, 891–900.

Palanivel, R., Koshy, P.M., and Murugan, N. (2011). *Development of mathematical model to predict the mechanical properties of friction stir welded AA6351 aluminum alloy.* Journal of Engineering Science and Technology Review, 4, 1, 25–31.

Periyasamy, P., Mohan, B., Balasubramanian, V., Rajakumar, S., and Venugopal, S. (2013). *Multiobjective optimization of friction stir welding parameters using desirability approach to join Al/SiCp metal matrix composites.* Transactions of Nonferrous Metals Society of China, 23, 4, 942–955.

Sabry, I. (2019). *Improvement of Mathematical Model to Predict the Mechanical Properties and Corrosion rate of Friction Stir Welded 2024 Aluminum Alloy.* in 2th International Conférence on Materials Science and Engineering, Cairo, Egypt, 11–13 March 2019.

Sabry, I. and El-Kassas, A. (2019). *An appraisal of characteristic mechanical properties and microstructure of friction stir welding for Aluminium 6061 alloy – Silicon Carbide SiCp metal matrix composite.* Journal of Mechanical Engineering and Sciences, 13, 4, 5804–5817.

Sabry, I., Mourad, A., and Thekkuden, D.T. (2020). *Optimization of metal inert gas welded aluminium 6061 pipe parameters using analysis of variance and grey relational analysis.* SN Applied Sciences, 2, 175, 1–11.

Sabry Abdel, H.I.M. and Thekkuden, D.T. (2021). *Vibration-Assisted friction stir welding of AA2024-T3 plates.* Proceedings of the ASME 2021 Pressure Vessels & Piping Conference PVP, July 12–16, online.

Sabry, I., Idrisi, A.H., and Ismail Mourad, A-H. (2021). *Friction stir welding process parameters optimization through hybrid multi-criteria decision-making approach.* International Review on Modelling and Simulations (IREMOS), 14, 1, 32–43.

Sathari, N.A.A., Shah, L.H., and Razali, A.R. (2014). *Investigation of single-pass/double-pass techniques on friction stir welding of aluminium.* Journal of Mechanical Engineering and Sciences, 7, 1053–1061.

Sheikh-Ahmad, J., Ozturk, F., Jarrar, F., and. Evis, Z. (2016). *Thermal history and microstructure during friction stir welding of Al–Mg alloy.* International Journal of Advanced Manufacturing Technology, 86, 1071–1081.

Stojanovic, B., Bukvic, M., and Epler, I. (2018). *Application of Aluminum and Aluminum Alloys in Engineering.* Applied Engineering Letters, 3, 2, 52–62.